ACS APPLIED ENERGY MATERIALS

www.acsaem.org Article

Quantitative Effects of Disorder on Chemically Modified Amorphous Carbon Electrodes

Debanjan Dhar,[‡] Catherine G. McKenas,[‡] Chiung-Wei Huang, Joanna M. Atkin,* Jillian L. Dempsey,* and Matthew R. Lockett*

Cite This: *ACS Appl. Energy Mater.* 2020, 3, 8038–8047 Read Online

ACCESS | Metrics & More | Article Recommendations | Supporting Information

ABSTRACT: Real materials are disordered. This disorder influences the properties of these materials and the chemical processes that occur at their interfaces. Gaining a molecular-level understanding of the underlying physical manifestations caused by disordered materials is crucial to unraveling and ultimately controlling the efficiency and performance of these materials in a range of energy-related devices. This understanding necessitates measurement techniques through which disorder can be detected, quantified, and monitored. However, such quantitative measurements are notoriously difficult, as effects often average out in ensemble measurements. In this work, we describe how a combination of electrochemical and spatially resolved surface spectroscopy measurements illuminate a molecular-level picture of disorder in materials. Using amorphous carbon as an intrinsically disordered material, we covalently attached a monolayer of ferrocene. Interfacial electron transfer across the amorphous carbon−ferrocene interface is highly sensitive to disruptions of order. By systematically varying linker properties and surface loadings, the influence of lateral interactions between nonuniformly distributed ferrocene headgroups on ensemble electrochemical measurements is demonstrated. Electrochemical and imaging data collectively indicate that conformational flexibility of the ferrocene moieties provides a mechanism to elude repulsive and unbalanced lateral interactions, while rigid linkages provide direct information about the underlying disorder of the material. This study is the first of its kind to quantify and visualize molecular disorder and heterogeneity with an experimental model accessed through ensemble measurements.

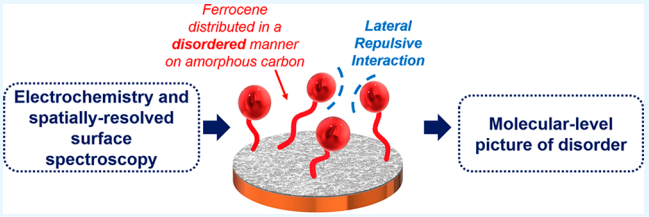

KEYWORDS: *amorphous carbon, disorder, electrochemistry, surface chemistry, surface-based spectroscopy*

INTRODUCTION

The micro- and nanoscale structure of a material can influence its interfacial properties and reactivity, ranging from wettability and adhesion to electron transfer kinetics and catalytic activity. Terms such as disorder and heterogeneity are often invoked to explain material interfaces with higher-than-expected reaction efficiencies or an unforeseen stability (or instability).[1−10] While disorder is viewed as a nebulous concept, it is generally recognized that the intrinsic disorder of a material or its interface can increase the material's overall functionality.[11]

If a material's functionality is related to disorder at its surface, strategically controlling this disorder should enable the rational design of functional materials.[12] The realization of this strategy is challenging given that measuring and quantifying disorder is notoriously difficult, as effects often average out in ensemble measurements.[13] Recognizing these challenges, we sought to explicitly quantify the effects of disorder on chemically modified amorphous carbon (aC) films, a material with intrinsic structural and chemical disorder. The recent characterization of atomically thin monolayers of aC highlights that there is a complete absence of long-range periodicity within this structure and a wide range of bond lengths, bond angles, and ring sizes present.[14] In the three-dimensional aC films explored in this work, similar extended disorder of the carbon network is predicted.[15,16] The high percentage of sp^2-hydbridized carbons in the aC films enables their covalent functionalization with redox-active ferrocene (Fc)-containing molecules, which provide an electrochemical probe to assess its underlying disorder. The monolayers of Fc formed on aC are starkly different from self-assembled monolayers (SAMs) of alkanethiols on gold, which are well-ordered structures that lead to outstanding electron transfer properties and experimental data in almost perfect congruence with predicted ideal theoretical behavior.[17−19]

Nonideal electron transfer behavior has been observed previously in ferrocene-containing monolayers that are unable to self-assemble, including covalently modified diamond,[20−22] glassy carbon,[23,24] amorphous carbon,[25,26] carbon nanofibers,[27] silicon,[28,29] and metal oxide surfaces.[30−32] Data-driven

Received: June 22, 2020
Accepted: July 6, 2020
Published: July 27, 2020

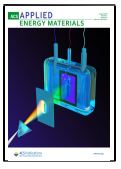

https://dx.doi.org/10.1021/acsaem.0c01434
ACS Appl. Energy Mater. 2020, 3, 8038–8047

Scheme 1. General Synthetic Route for the aC-$(CH_2)_n$-Fc (n = 0, 2, 6, 11) Films[a]

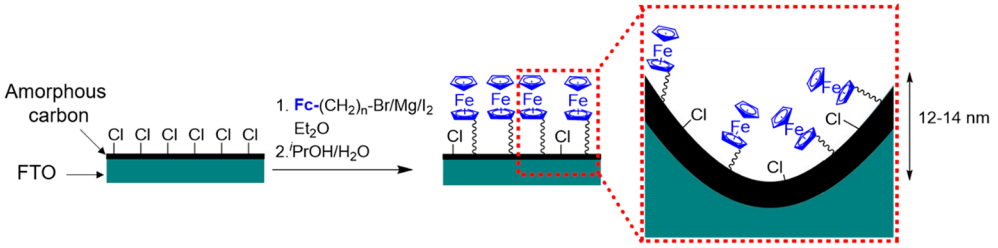

[a]The zoom-in on the right is curved to emphasize the underlying roughness of the amorphous carbon.

explanations for these observations have not yet been presented, but hypotheses for this nonideality include the uncompensated resistance of the film, the insulating nature of the appended monolayer, and lateral interactions between the surface-anchored electroactive head groups. Here, we examine if macroscale electrochemical measurements can provide a molecular-level picture of disorder. By coupling electrochemical measurements to spatially resolved Kelvin probe force microscopy (KPFM), atomic force microscopy (AFM), and micro-Raman spectroscopy, we elucidate the chemical and electronic disorder of these modified materials and draw conclusions about the role of disorder at a molecular level. We then correlate observed macroscopic electron transfer properties to the structure of these covalently modified electroactive thin films. To the best of our knowledge, this is the first study to systematically assess the effect of disorder on macroscopic chemical properties of covalently modified thin films by changing a single variable—the ability of the ferrocene molecules to reorient themselves spatially on the surface—and illuminate a molecular-level picture of disorder from ensemble measurements.

RESULTS AND DISCUSSION

Generation and Characterization of Ferrocene-Terminated aC Surfaces. Amorphous carbon films are an intrinsically disordered material, with a topography that is not atomically smooth and a chemical composition containing a mixture of hybridization states. Experimental and computational studies demonstrate that energy of adsorption, chemical reactivity, and optical properties of these films can be modulated by simply altering the ratio of sp^2- and sp^3-hybridized carbons, an experimental parameter that can be controlled during deposition.[15,33,34] The aC films used in this work were prepared from DC magnetron sputtering a graphite source onto fluorine-doped tin oxide (FTO)-coated slides, retaining the conductivity of the FTO but providing the stability of a carbon surface. These films have been characterized in depth previously. They are largely sp^2 in nature as determined by XPS and optical bandgap measurements, with trace amounts of oxidized carbon species.[26]

To prepare the aC-$(CH_2)_6$-Fc films used in this work, Grignard reagents of Fc-$(CH_2)_6$-Br were generated in the presence of chlorine-terminated (aC-Cl) films, using Mg and I_2 (Scheme 1). To determine the selectivity of this reaction, we performed two controls. First, we treated aC-Cl films with Fc-$(CH_2)_6$-Br and Mg, in the absence of I_2. Second, we treated aC-H films with Fc-$(CH_2)_6$-Br in the presence of Mg and I_2. X-ray photoelectron spectra of both aC-Cl surfaces contained an Fe(II) 2p doublet at 708 and 720 eV, indicating surface immobilized Fc (Figure S1 and Table S1).[35−37] The intensity of the Fe(II) signals for the aC-Cl surfaces in the absence of iodine was ∼40% lower, confirming its importance in the reaction. The aC-H films contained no Fe(II) signal. More quantitative values of surface loading (Γ) obtained from integration of the charge passed in cyclic voltammograms supported the XPS results, with values of $\Gamma = 1.24(3) \times 10^{-9}$ and $\Gamma = 1.21(5) \times 10^{-10}$ mol/cm^2 of ferrocene in the presence and absence of I_2, respectively. We generated films with intermediate surface loadings by modulating reaction time and Fc-$(CH_2)_6$-Br concentration. Using similar reaction conditions, we also attached Fc-$(CH_2)_n$-Br molecules with alkyl chain linker lengths of n = 0, 2, and 11.

The Fc surface loading in the I_2-catalyzed Grignard reaction is comparable, and in some cases surpasses, previously reported coverages on carbon-based materials.[20,22,26,27,38−42] We postulate this high surface loading is a consequence of both the film and the modification chemistry. The chemical composition and topography of the aC films results in a large number of reactive surface sites. Further, the highly reactive Grignard reagent incorporates the ferrocene molecules onto aC-Cl films in a one-step reaction. To characterize the topography and chemical composition of the aC films, we used AFM (Figure S2) and micro-Raman spectroscopy (Figure S3). The AFM-measured surface area is ∼15−20% higher than its geometric surface area (Table S2) with root-mean-squared (RMS) roughness values of 12−14 nm. The films contained the diagnostic I_D and I_G Raman peaks (Figure S3), with an intensity ratio between 0.50−0.56. This sp^2-to-sp^3 carbon ratio agrees with our previous characterizations of the films[26] and supports the high surface loading, as sp^2-hybridized carbons present at graphitic edge planes are known to be the reactive sites in carbon-based materials.[43] The AFM (Figure S2) and micro-Raman measurements (Figure S3) also show chemical modification did not alter the topography or composition of the aC film. The stability of the surface allowed us to attribute conclusions about observed heterogeneity in electron transfer processes to the heterogeneity of the Fc monolayer imparted by the underlying disorder of the aC.

Cyclic Voltammetric Analysis of aC-$(CH_2)_n$-Fc. Cyclic voltammograms of the aC-$(CH_2)_6$-Fc films contain diagnostic electrochemical features (Figure 1) but have significant deviations from the canonical voltammograms anticipated for surface-confined electroactive compounds: a ΔE_p = 0 and peaks with full-width at half-maximum (fwhm) values of 90.6 mV.[44,45] Here, ΔE_p is defined as the difference between the anodic (E_{pa}) and cathodic (E_{pc}) peak potentials. For aC-$(CH_2)_6$-Fc samples with a $\Gamma = 1.24(3) \times 10^{-9}$ mol/cm^2, the ΔE_p is 60 mV and the fwhm value is ∼130 mV at a scan rate of 200 mV/s. A 10-fold decrease in surface loading ($\Gamma = 1.21(5) \times 10^{-10}$ mol/cm^2) has a ΔE_p of 15 mV and fwhm ∼115 mV,

https://dx.doi.org/10.1021/acsaem.0c01434
ACS Appl. Energy Mater. 2020, 3, 8038−8047

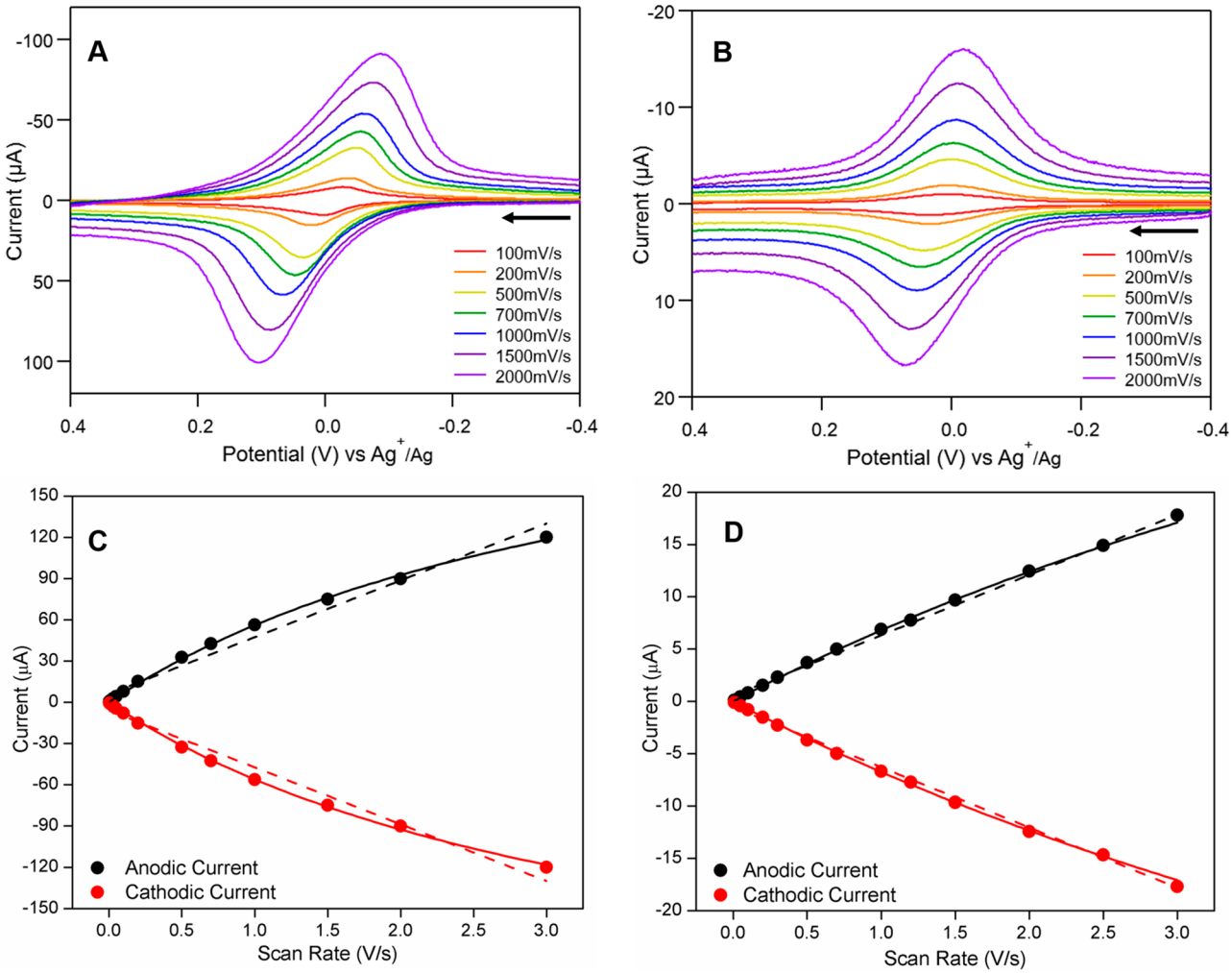

Figure 1. Scan rate-dependent voltammograms (100−2000 mV/s) for (A) $\Gamma = 1.24(3) \times 10^{-9}$ mol/cm^2 and (B) $\Gamma = 1.21(5) \times 10^{-10}$ mol/cm^2 aC-$(CH_2)_6$-Fc films. Voltammograms recorded in 0.25 M $[Bu_4N][PF_6]$ acetonitrile solution. Peak current vs scan rate data for (C) $\Gamma = 1.24(3) \times 10^{-9}$ mol/cm^2 and (D) $\Gamma = 1.21(5) \times 10^{-10}$ mol/cm^2 samples. Each point represents the baseline-corrected peak current at a given scan rate. The solid trace depicts the experimental data fit to eq 1, while the dashed trace depicts a linear fit.

indicating increased surface loading causes enhanced deviations from ideal electrochemical behavior. Similar deviations from ideality have been observed on diamond, gold, and silicon surfaces with covalently anchored Fc.[20,46−48] It has been postulated that surface-anchored electroactive species can experience nonuniform local environments arising from substantial electrostatic interactions, strong dipole−dipole interactions or high mobility.[49,50] The presence of such lateral interactions results in broader peaks for molecules experiencing repulsive interactions and narrower peaks for attractive interactions. Increases in surface loading are expected to accentuate the effects of repulsive lateral interactions and are consistent with our observations.

Plotting peak current (anodic and cathodic) as a function of scan rate, we observe deviation from the anticipated linear relationship for ideal cases. These deviations increase with increased surface loading (Figure 1).[51] This relationship was not observed in the non-Faradaic charging current, indicating that decreased ionic mobility at high surface loading is not contributing to these deviations from ideality (Figure S4).[52] Laviron predicted such deviations for surface-bound species with repulsive lateral interactions and moderate heterogeneous electron transfer kinetics,[49] generalizing the relationship with eq 1

$$i = \frac{n^2F^2A\Gamma v^x}{4RT\left(1 - \frac{G\theta}{2}\right)} \quad (1)$$

where i = peak current, n = number of electrons transferred, A = surface area, υ = scan rate, F = Faraday constant, R = gas constant, T = temperature, x = variable exponent of 0−1, and $G\theta$ = lateral interaction parameter of the immobilized species. The $G\theta$ value is negative for repulsive interactions and positive for attractive interactions. The x value is less than 1 when the electron transfer kinetics are moderately slow, but expected to be 1 when the electron transfer kinetics are fast.[49] When we fit baseline-corrected peak current data to eq 1 (Figure 1), $G\theta = -5.45(3)$ and $x = 0.725(1)$ for $\Gamma = 1.24(3) \times 10^{-9}$ mol/cm^2. The low surface loading ($\Gamma = 1.21(5) \times 10^{-10}$ mol/cm^2) film is best fit with $G\theta = -2.52(4)$ and $x = 0.945(3)$. In both cases, the negative $G\theta$ value indicates repulsive lateral interactions between the surface-anchored Fc moieties with significantly more repulsions in the higher surface loading films. Moreover, the value of x for the higher surface loading film is significantly lower than unity, indicating significant deviations from ideality.

https://dx.doi.org/10.1021/acsaem.0c01434
ACS Appl. Energy Mater. 2020, 3, 8038−8047

To confirm the repulsive interaction parameter varies as a function of Fc surface loading, we repeated the same analysis for aC-$(CH_2)_6$-Fc samples with $\Gamma = \sim 9 \times 10^{-12}$ to $\sim 1 \times 10^{-9}$ mol/cm^2. The negative $G\theta$ values (Table 1) indicate repulsive

Table 1. Variation of the Lateral Interaction Parameter with Surface Loading of Ferrocene for aC-$(CH_2)_6$-Fc Films[a]

surface loading (mol/cm^2)	$G\theta$	x
$9.15(2) \times 10^{-12}$	−1.31(6)	0.938(6)
$1.21(5) \times 10^{-10}$	−2.52(4)	0.945(3)
$2.15(2) \times 10^{-10}$	−3.51(7)	0.872(6)
$7.85(2) \times 10^{-10}$	−4.45(3)	0.784(3)
$1.24(3) \times 10^{-9}$	−5.45(3)	0.725(1)

[a]Values, which are the average of two measurements from separate regions of the same sample, are determined from charge integration of voltammograms at a scan rate of 100 mV/s. For $\Gamma = 1.24(3) \times 10^{-9}$ mol/cm^2, the charge integration is at 2 mV/s (Figure 2C).

lateral interactions between the Fc moieties. The absolute magnitude of $G\theta$ increases with increasing surface loading, varying from −1.31(6) for $\Gamma = 9.15(2) \times 10^{-12}$ mol/cm^2 to −5.45(3) for $\Gamma = 1.24(3) \times 10^{-9}$ mol/cm^2. A similar trend is also observed in the x value, which increases with decreasing surface loading, ultimately plateauing out at ∼0.94 for the two lowest surface loading films. This trend corroborates the hypothesis that the extent of the repulsive interaction increases with increasing surface loading. These repulsive interactions give rise to significant deviations from idealized electrochemical behavior for the high surface loading films, leading to slower electron transfer kinetics (Figure S5).

Ruther et al. demonstrated that the conformational flexibility of alkyl chains in Fc-triazole-$(CH_2)_n$ (n = 4, 6, 11) monolayers tethered to diamond electrodes allowed the Fc to dynamically approach the surface at low surface densities ($\Gamma \sim 10^{-11}$ mol/cm^2), resulting in facile electron transfers.[20] To determine if the conformational flexibility of the $-(CH_2)_6-$ linker in our study was mitigating the electrostatic repulsions at lower surface loadings, we prepared films with varying linker lengths: aC-$(CH_2)_n$-Fc, where n = 2, 6, and 11. At $\Gamma = \sim 10^{-10}$ mol/cm^2, the voltammograms of aC-$(CH_2)_{11}$-Fc exhibit more idealized behavior than for n = 2 or 6 (Figure 2A), with the lowest ΔE_p and fwhm values (Table 2 and Figure 2A). The $G\theta$ values are also linker length-dependent, with the most negative value for the shortest alkyl chain and least negative for the longest alkyl chain. These trends corroborate the hypothesis that increasing the flexibility of the alkyl chain results in decreased repulsive lateral interactions between the Fc moieties.

Cyclic voltammograms of the highest surface loading aC-$(CH_2)_6$-Fc film ($\Gamma = 1.24(3) \times 10^{-9}$ mol/cm^2) contain a second anodic peak at a slightly positive potential at scan rates of 2−50 mV/s (Figure 2B). The peak height of this second anodic feature decreases with increasing scan rate. Interestingly, the cumulative anodic charge passed also decreases with increasing scan rate and is unchanged for scan rates >500 mV/s (Figure 2C). Ideally, the charge passed in the voltammograms of surface-tethered species is independent of the scan rate, which is in fact the case for the lower density, $\Gamma = 1.21(5) \times 10^{-10}$ mol/cm^2 aC-$(CH_2)_6$-Fc films (Figure 2C). We hypothesize that the increasing numbers of Fc^+ formed during the anodic scan result in repulsive electrostatic interactions large enough to cause the head groups of neighboring

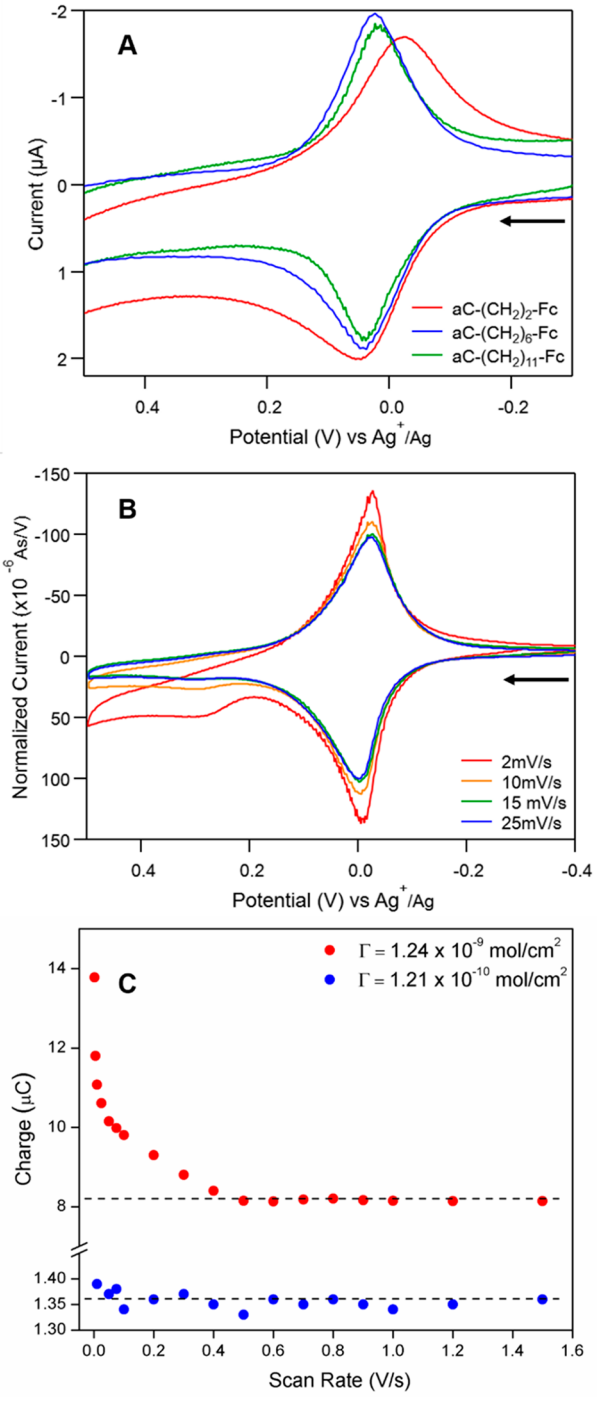

Figure 2. (A) Cyclic voltammograms (scan rate = 100 mV/s) for aC-$(CH_2)_2$-Fc (red), aC-$(CH_2)_6$-Fc (blue) and aC-$(CH_2)_{11}$-Fc (green) recorded at comparable surface coverages (Table 2). (B) Scan rate-normalized voltammograms for aC-$(CH_2)_6$-Fc ($\Gamma = 1.24(3) \times 10^{-9}$ mol/cm^2) films. Voltammograms recorded in 0.25 M $[Bu_4N][PF_6]$ acetonitrile solution. (C) Anodic charge passed in the voltammograms at $\Gamma = 1.24(3) \times 10^{-9}$ mol/cm^2 (red) and $\Gamma = 1.21(5) \times 10^{-10}$ mol/cm^2 (blue) for aC-$(CH_2)_6$-Fc films as a function of scan rate; the dashed black line depicts the charge plateau. Note y-axis scales are different for the two films.

ferrocenes to reposition, a movement that is made possible by the flexibility of the alkyl chain. In cases where the surface loading is low, this dynamic process is favorable. In cases where the surface loading is high, this repositioning becomes

https://dx.doi.org/10.1021/acsaem.0c01434
ACS Appl. Energy Mater. 2020, 3, 8038−8047

Table 2. Key Parameters for the aC-$(CH_2)_n$-Fc Films

n	surface loading (mol/cm^2)[a]	ΔE_p at 100 mV/s (mV)	fwhm (mV)	$G\theta$	x
2	$1.95(3) \times 10^{-10}$	70	150	−5.36(8)	0.646(8)
6	$2.15(2) \times 10^{-10}$	20	110	−3.51(7)	0.872(6)
11	$1.82(4) \times 10^{-10}$	20	100	−1.82(6)	0.864(4)

[a]Values, which are the average of two measurements from separate regions of the same film, are determined from charge integration of voltammograms at a scan rate of 100 mV/s.

progressively more unfavorable, and the electron transfer kinetics are significantly attenuated for a fraction of the Fc molecules on the surface. As a result, approximately 40% of the surface-bound Fc species are not oxidized under standard voltammetry conditions, as evidenced by the drop in charge passed from ∼14−8.5 μC (Figure 2C). At very slow scan rates, this kinetically sluggish but thermodynamically unfavorable process is observed, resulting in a positive shift of ∼200 mV for the second anodic peak. We posit that as Fc^+ is reduced back to Fc during the cathodic scan, repulsive interactions are reduced, and reduction of all Fc^+ moieties can occur without substantial overpotential, leading to the observation of only one cathodic peak.

Kinetic Consequences of Lateral Interactions. To establish how lateral interactions affect electron transfer rate constants, we measured the heterogeneous electron transfer rate constant (k_s) between Fc and aC surface at different surface loadings of aC-$(CH_2)_6$-Fc. Typically, k_s values are estimated by analyzing overpotential as a function of scan rate.[45,50] Kinetic dispersion occurs in the aC-$(CH_2)_6$-Fc samples, as evidenced by nonsingle exponential Faradaic charging current decays (Figure S6).[46−48] Nevertheless, the k_s values estimated using Laviron's analysis are 14 s^{-1} for Γ = $1.24(3) \times 10^{-9}$ mol/cm^2 and 25 s^{-1} for Γ = $1.21(5) \times 10^{-10}$ mol/cm^2. While these values fail to account for different local environments within the electroactive monolayer that should give rise to a range of k_s values,[46−49] they do qualitatively illustrate that measured rate constants decrease with increasing surface loading (Figure S7).

To obtain more quantitative estimates of the k_s values, we used electrochemical impedance spectroscopy (EIS). The impedance of aC-$(CH_2)_6$-Fc films was measured at the $E_{1/2}$ (∼0.04 V vs Ag^+/Ag) between a frequency range of 1 Hz and 1 MHz. A representative Bode plot for aC-$(CH_2)_6$-Fc (Γ = $1.24(3) \times 10^{-9}$ mol/cm^2) is shown in Figure 3B. The data was modeled with a Debye equivalent circuit (Figure 3A).[20,51,53,54] The circuit, which is ideal for modeling the impedance of an electrode containing a redox-active monolayer, consists of a solution cell resistance (R_{SOL}), double layer capacitance (C_{DL}), charge-transfer resistance of the thin film (R_{CT}), and capacitance of the thin film (C_{AD}). The electron transfer rate constant is determined with the relation $k_s = 1/(2\ R_{CT}C_{AD})$ (Table 3).[42,53] The value of R_{SOL}, which is expected to depend on the electrolyte concentration and electrode geometry, does not vary between samples (250−270 Ω).

The capacitance of both the thin film and the double layer increase with surface loading, consistent with an increased overall charge on the thin films. Most notably, k_s values are substantially higher at lower surface loading. These observations agree with Ruther et al.,[20] who attributed the enhanced electron transfer kinetics at lower surface loadings to the ease at which the Fc moieties could approach the electrode surface.

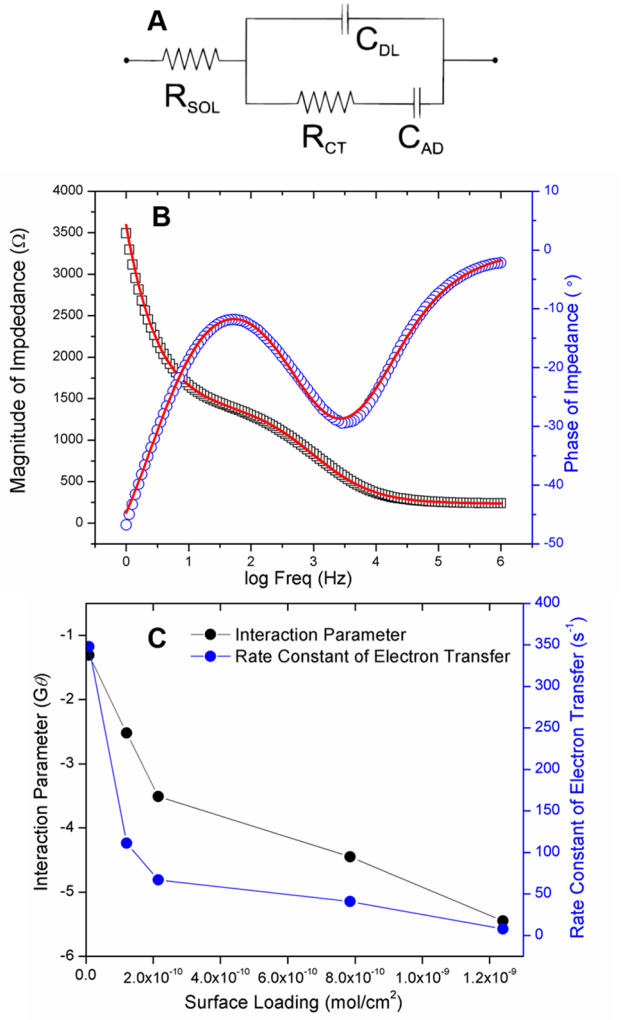

Figure 3. (A) Debye equivalent circuit used to model surface-anchored electroactive species on the aC films. (B) Illustrative Bode plot for aC-$(CH_2)_6$-Fc (Γ = $1.24(3) \times 10^{-9}$ mol/cm^2) showing the experimentally observed magnitude (black square) and phase (blue circle) in the EIS measurements, with the fits depicted as the red trace (bottom left). EIS measurements in acetonitrile solvent containing 0.25 M $[Bu_4N][PF_6]$. (C) Correlations between $G\theta$ and surface loading (black), as well as k_s and surface loading (blue), for different aC-$(CH_2)_6$-Fc films.

Table 3. Parameters from Impedance Fits

surface coverage (mol/cm^2)	C_{DL} (μF)	C_{AD} (μF)	R_{CT} (kΩ)	k_s (s^{-1})
$9.15(2) \times 10^{-12}$	1.497	1.296	1.108	348
$1.21(5) \times 10^{-10}$	1.742	3.586	1.245	111
$2.15(2) \times 10^{-10}$	2.933	6.295	1.187	67
$7.85(2) \times 10^{-10}$	4.458	9.672	1.256	41
$1.24(3) \times 10^{-9}$	4.832	48.15	1.332	8

Their results differ from the current study in two aspects: the electron transfer rate constants are significantly higher (10^3−10^4 s^{-1}) and the voltammograms do not depict significant deviation from ideality. These differences are likely due to a ∼10-fold lower surface loading, supporting the notion that increased surface loading results in increased repulsive lateral interactions of electroactive species, enhanced deviation from ideality, and decreased electron transfer kinetics.

https://dx.doi.org/10.1021/acsaem.0c01434
ACS Appl. Energy Mater. 2020, 3, 8038−8047

Voltammetric Peak Splitting Is Due to the Disordered Distribution of Surface-Bound Redox Sites. The relationship between peak current and scan rate formulated by Laviron (eq 1) assumes surface-bound species are uniformly distributed. Matsuda et al. postulated that the presence of lateral interactions is not consistent with this assumption and interactions between the surface-anchored species are accompanied by disorder (nonrandomness) in the distribution of the surface anchored species.[55,56] The accompanying theoretical model predicts that combining a high degree of repulsive lateral interactions with a disordered distribution of the electroactive species will result in voltammetric peak splitting. By contrast, when the extent of repulsive interactions is low, a broad peak is observed at the middle of the split peaks.

We postulate the covalent attachment method used to functionalize aC gives rise to a disordered distribution of surface-bound electroactive species, but no peak splitting was observed in aC-$(CH_2)_n$-Fc (n = 2, 6, 11). We hypothesize that conformational flexibility may mask these lateral interactions that give rise to peak splitting on both the anodic and cathodic scans. To test this notion, we immobilized Fc directly on the surface using Fc-Br as the Grignard precursor. We generated aC-Fc films with a high and low surface loading using our previously established Grignard protocol with and without I_2, respectively. Voltammograms of high surface loading (Γ = 1.58(5) × 10^{-10} mol/cm^2) films exhibit the predicted peak splitting in both the anodic and cathodic branches for scan rates of 50−1000 mV/s (Figure 4A). At scan rates of >1500 mV/s, the two distinct redox features merge into a broad peak. When the baseline-corrected peak currents for the two anodic peaks of the voltammograms are plotted as a function of scan rate, a nonlinear dependence is also observed (Figure S8). The fit obtained from the plot of the cumulative anodic peak height vs scan rate yields $G\theta$ = −7.13(5) and x = 0.752(8), indicating the presence of extensive repulsive lateral interactions between the Fc groups.

In the low surface loading aC-Fc films (Γ = 1.7(4) × 10^{-11} mol/cm^2), the voltammogram has a single broad feature with a fwhm ∼140 mV (Figure S9). The corresponding E_{pa} and E_{pc} values are approximately in the middle of the split peaks observed for the high surface loading films (Figure 4B, Figure S9). The baseline corrected peak current vs scan rate data depict a nonlinear dependence yielding $G\theta$ ∼ −5.5 and x ∼ 0.75 (Figure S10), indicating lower repulsive lateral interactions than at high surface loading. Our experimental observations are in agreement with the theoretical predictions of peak splitting arising from nonuniform lateral interactions between the electroactive species proposed by Matsuda et al.[55,56] Crucially, split peaks in the voltammetric response are observed across a range of scan rates for the high surface loading aC-Fc, while a single broad peak is observed when the lateral interactions are attenuated by lowering surface loading. These observations are also in congruence with the hypothesis that the surface distribution of Fc is indeed disordered. We posit that the absence of a flexible alkyl chain severely accentuates these interactions even at low surface coverages, particularly when the Fc moieties are in close proximity to each other or to the surface and thus explicit detection of underlying aC disorder in bulk measurements is only achievable when this flexibility is eliminated.

Probing the Nature of the Disordered Distribution of Surface-Anchored Fc. We considered two possible distributions of surface-anchored Fc that would give rise to the

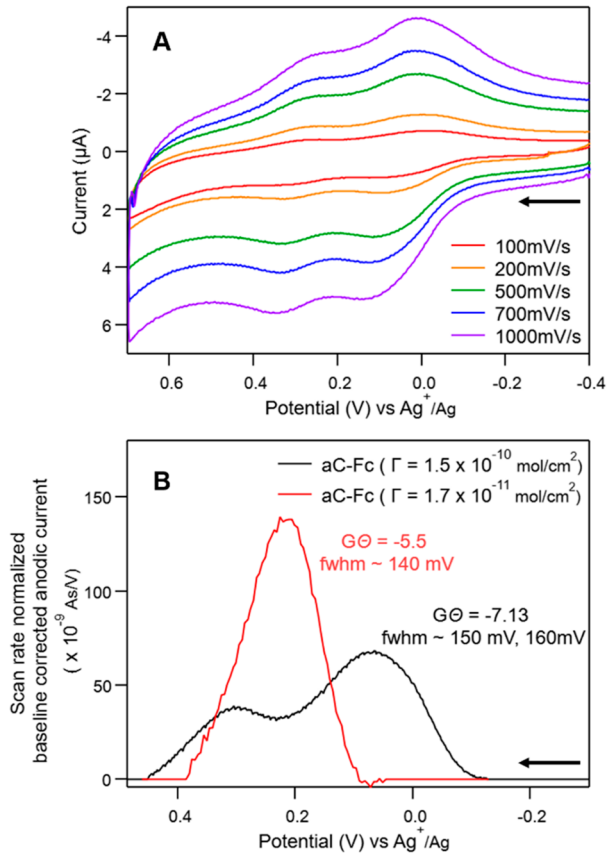

Figure 4. (A) Cyclic voltammograms for an aC-Fc film (Γ ∼ 1.5 × 10^{-10} mol/cm^2) at scan rates of 100−1000 mV/s. (B) Scan rate normalized, baseline corrected anodic peaks for aC-Fc film (Γ = 1.58(5) × 10^{-10} mol/cm^2, black trace) and for aC-Fc film (Γ = 1.7(4) × 10^{-11} mol/cm^2, red trace). Voltammograms recorded at 100 mV/s in 0.25 M $[Bu_4N][PF_6]$ acetonitrile solution.

density- and linker-dependent lateral interactions we observed: (1) islands of closely spaced Fc distributed across the surface in a disordered manner or (2) an unevenly spaced distribution of Fc over the entire surface. Clustered domains of Fc in two-component SAMs of methyl- and Fc-terminated alkanethiols on gold give rise to peak splitting at slow scan rates (20 mV/s).[57] One peak is attributed to isolated Fc moieties and the other to clustered islands of Fc. The clustered islands, which are predominant at high surface loadings, led to sharp peaks with fwhm values of <90.6 mV. We did not observe such effects on aC films, and the >90.6 mV fwhm values we observe suggest that the Fc groups are not clustered together and are likely distributed nonuniformly across the surface.

To provide additional evidence in favor of the nonuniform distribution of Fc molecules on the surface, we drew inspiration from studies on partially blocked electrodes,[58] which have two limiting regimes: (1) blocked islands and (2) uniformly blocked electrodes. In the blocked island case, a decrease in the effective surface area leads to lower currents, but similar electron transfer kinetics to an unmodified electrode when analyzing diffusional electrochemical species. In the blocked electrode case, a significant decrease in electron transfer rates is due to electrode modification. To replicate the blocked electrode scenario, we generated redox inactive aC films by attaching CH_3-$(CH_2)_5$-Br. Cyclic voltammograms of freely diffusing Fc have ΔE_p > 400 mV at scan rates as low as 50 mV/s, without significant loss of current intensity (peak

https://dx.doi.org/10.1021/acsaem.0c01434
ACS Appl. Energy Mater. 2020, 3, 8038−8047

height) when compared to unmodified aC films (Figure S11). This considerable decrease in the heterogeneous electron transfer rate constant ($\Delta E_{p,ideal}$ = 57 mV on aC)[26] supports a surface on which Fc is distributed without local order (Figures S12 and 5).

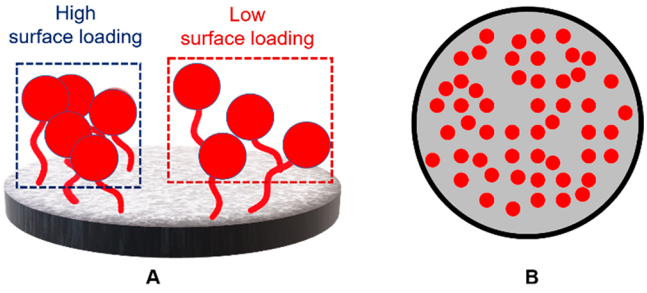

Figure 5. (A) Schematic diagram of aC-$(CH_2)_n$-Fc showing the surface distribution of Fc for a high surface loading with a flexible alkyl chain (left) and a low surface loading with a flexible alkyl chain linker that allows the Fc molecules to dynamically approach the surface (right). (B) Two-dimensional projection of the top view of the functionalized aC electrode showing the nonrandom distribution of Fc molecules on the surface.

Spatially resolved Kelvin probe force microscopy (KPFM) of the functionalized aC films further support a nonuniform distribution of Fc. Attaching Fc to the surface lowers the work function of aC-Cl films, resulting in an anticipated trend of Φ = aC-Cl > aC-$(CH_2)_6$-Fc (high loading) > aC-$(CH_2)_6$-Fc (low loading) > aC-Fc (Figure 6), as the Fc replaces the electronegative chlorines. The magnitude of this decrease should be dependent on the proximity of the Fc to the surface and supports rearrangement of the Fc molecules at low surface loadings. An arrangement where Fc moieties lie flat on the surface would give rise to a work function closer to aC-Fc. The higher surface loading aC-$(CH_2)_6$-Fc films ($\Gamma \sim 1 \times 10^{-9}$ mol/cm^2) have the largest range of the work function values (Figure 6), consistent with the notion that high packing significantly hinders the conformational flexibility of the molecules. The corresponding AFM images indicate the underlying surface topography is not contributing to these variations (Figure S2). To further gauge the spatial distribution of the Fc on the surface, we performed correlation length analysis to estimate the spatial periodicity of the work function variations. Spatial correlation provides a measure of how much the work function changes across different length scales within the samples. The analysis yields values of 45 nm for aC-Cl, 64 nm for aC-$(CH_2)_6$-Fc with $\Gamma \sim 10^{-9}$ mol/cm^2, 72 nm for aC-$(CH_2)_6$-Fc with $\Gamma \sim 10^{-10}$ mol/cm^2, and 96 nm for aC-Fc with $\Gamma \sim 10^{-10}$ mol/cm^2. The length scale for the aC-Fc is notable; in the absence of conformational flexibility, the large distance indicates that the regions of low and high work function are distributed across the surface and not clustered together, suggesting the regions where Fc is attached on the surface are distributed across the surface.

CONCLUSION

While disorder and chemical heterogeneity abound at chemical interfaces, few studies have accurately measured or elucidated their effects on macroscopic system properties. In this work, we show that installation of redox-active Fc groups on the surface of aC films provides an electrochemical probe to interrogate the intrinsic disorder of this material. The aC film

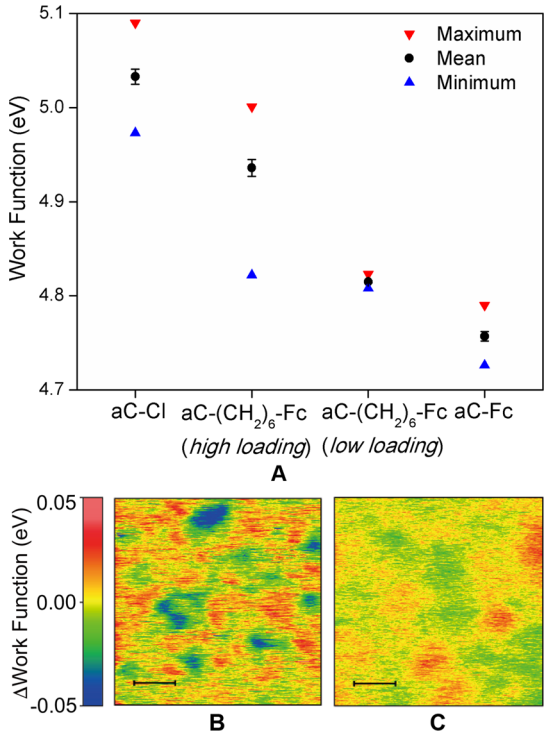

Figure 6. (A) Work functions of four different aC samples showing the maximum (downward triangle), minimum (upward triangle), and mean (circle, error bars denote the standard deviation) work function values, obtained from KPFM measurements. aC-$(CH_2)_6$-Fc (*high loading*) corresponds to a $\Gamma \sim 10^{-9}$ mol/cm^2 and aC-$(CH_2)_6$-Fc (*low loading*) corresponds to a $\Gamma \sim 10^{-10}$ mol/cm^2. Representative KPFM images of (B) aC-$(CH_2)_6$-Fc ($\Gamma \sim 10^{-9}$ mol/cm^2) and (C) aC-Fc ($\Gamma \sim 10^{-10}$ mol/cm^2) films. The maps are plotted as the deviation from the mean work function, denoted by ΔWork Function, in order to compare the magnitude of variations across different samples. Scale bar = 200 nm.

has chemical heterogeneity arising from the presence of both sp^3- and sp^2-hybridized carbons, and spatial heterogeneity conveyed by the intrinsic roughness of the aC film. Covalent attachment of ferrocene to these films is enabled by the high percentage of sp^2-hybridized carbons in the film, and their reaction with an in situ Grignard reagent to incorporate pendant Fc groups. Systematic exploration of surface loading and conformational flexibility reveals that lateral interactions between the Fc groups lead to nonidealities in the electrochemical behavior, which can be quantified through the lateral interaction parameter $G\theta$ and the heterogeneous electron transfer rate constant k_s. Correlations showing that lateral interactions increase with increasing surface coverages and decrease with linker flexibility support the conclusion that the disorder arises from the intrinsic chemical and spatial heterogeneity of the aC films. In the absence of a flexible linker, we observe a broad voltammetric response at low surface loading. This peak splits with increased surface loading. These observations are consistent with theoretical predictions in the case of disordered surface distribution of redox sites with repulsive lateral interactions. Electrochemical and spatially resolved KPFM measurements show that the disorder persists across the surface, rather than arising from ferrocene islands. KPFM measurements further show that Fc groups with alkyl-chain spacers and low surface loadings have more freedom to orient themselves to evade repulsive lateral interactions. We

https://dx.doi.org/10.1021/acsaem.0c01434
ACS Appl. Energy Mater. 2020, 3, 8038−8047

also found that lateral interactions between Fc groups give rise to subpopulations of Fc molecules that undergo oxidation at slower rates than others.

Our findings suggest that interfacial structure can have profound effects on how disorder manifests in material performance, and that our understanding of these effects is underpinned by the ability to use characterization tools to probe this structure. Here, for example, we found that flexibility of the linker tethering Fc to the aC surface can minimize the apparent effects of lateral interactions in electrocatalysis and obscure the effects of disorder. Further, our finding that voltammetry at high scan rates cannot accurately capture the full picture of electroactive groups in different microenvironments on a disordered surface shows that electrochemistry cannot be used to directly quantify surface coverage or turnover numbers for surface-immobilized catalysts on a highly disordered material. The influence of interfacial structure and disorder is applicable to surface chemistry in a broader respect, particularly when trying to design functional materials that involve modification of an interface. Multifaceted approaches to characterization are necessary to provide a clear picture of heterogeneous microenvironments that lead to altered reactivities.

While it has traditionally been thought that ensemble measurements average out effects of disorder, this work demonstrates clearly that disorder in materials can be explicitly detected and quantified through electrochemical measurements. The versatility of this methodology will enable more routine monitoring of disorder and heterogeneity in materials and ultimately provide access to an enhanced understanding of the role of disorder in driving performance for a myriad of functional materials. Elucidating the nonideal behavior of energy materials is the linchpin needed to improve their function and advance these materials for real-world applications.

■ ASSOCIATED CONTENT

Supporting Information

The Supporting Information is available free of charge at https://pubs.acs.org/doi/10.1021/acsaem.0c01434.

Experimental details, additional spectroscopic and electrochemistry data, and electrochemical cell schematics (PDF)

■ AUTHOR INFORMATION

Corresponding Authors

Joanna M. Atkin − *Department of Chemistry, University of North Carolina at Chapel Hill, Chapel Hill, North Carolina 27599-3290, United States;* orcid.org/0000-0002-1211-5193; Email: jatkin@email.unc.edu

Jillian L. Dempsey − *Department of Chemistry, University of North Carolina at Chapel Hill, Chapel Hill, North Carolina 27599-3290, United States;* orcid.org/0000-0002-9459-4166; Email: dempseyj@email.unc.edu

Matthew R. Lockett − *Department of Chemistry, University of North Carolina at Chapel Hill, Chapel Hill, North Carolina 27599-3290, United States;* orcid.org/0000-0003-4851-7757; Email: mlockett@email.unc.edu

Authors

Debanjan Dhar − *Department of Chemistry, University of North Carolina at Chapel Hill, Chapel Hill, North Carolina 27599-3290, United States;* orcid.org/0000-0002-3027-0226

Catherine G. McKenas − *Department of Chemistry, University of North Carolina at Chapel Hill, Chapel Hill, North Carolina 27599-3290, United States;* orcid.org/0000-0003-1118-2105

Chiung-Wei Huang − *Department of Chemistry, University of North Carolina at Chapel Hill, Chapel Hill, North Carolina 27599-3290, United States*

Complete contact information is available at: https://pubs.acs.org/10.1021/acsaem.0c01434

Author Contributions

‡D.D. and C.G.M. contributed equally.

Notes

The authors declare no competing financial interest.

■ ACKNOWLEDGMENTS

Electrode fabrication and modification was supported by the National Institutes of Health, National Institute of General Medical Sciences, under award number 5R35GM128697 (supporting C.G.M and M.R.L.); electrochemical analysis was supported by U.S. Department of Energy, Office of Science, Office of Basic Energy Sciences, under Award DE-SC0015303 (supporting D.D. and J.L.D); and surface characterization was supported by National Science Foundation Chemical Measurement and Imaging program, under Grant no. CHE-1848278 (supporting C.-W.H. and J.M.A.). We thank Kristina Herrera, James Taylor, Nicole Smiddy, Daniel Kurtz, Ludovic Troian-Gautier, and Jackson Hall for experimental assistance, Prof. Thomas Meyer for providing FTO substrates, Prof. Alexander Miller for access to a potentiostat, Prof. Kizhanipuram Vinodgopal for the use to the KPFM at North Carolina Central University, and Dr. Carrie Donley for surface-characterization instrumentation expertise and helpful conversations regarding data interpretation. Part of this work was performed at the Chapel Hill Nanofabrication and Analysis Laboratory, a member of the North Carolina Research Triangle Nanotechnology Network (RTNN), which is supported by the National Science Foundation, Grant ECCS-1542015, as part of the National Nanotechnology Coordinated Infrastructure (NNCI). J.L.D. acknowledges support from a Packard Fellowship for Science and Engineering and the Alfred P. Sloan Foundation. M.R.L. acknowledges support from Young Investigator Award from Eli Lilly and Company.

■ REFERENCES

(1) Wu, Y.; Okesola, B. O.; Xu, J.; Korotkin, I.; Berardo, A.; Corridori, I.; di Brocchetti, F. L. P.; Kanczler, J.; Feng, J.; Li, W.; Shi, Y.; Farafonov, V.; Wang, Y.; Thompson, R. F.; Titirici, M.-M.; Nerukh, D.; Karabasov, S.; Oreffo, R. O. C.; Carlos Rodriguez-Cabello, J.; Vozzi, G.; Azevedo, H. S.; Pugno, N. M.; Wang, W.; Mata, A. Disordered Protein-Graphene Oxide Co-Assembly and Supramolecular Biofabrication of Functional Fluidic Devices. *Nat. Commun.* **2020**, *11* (1), 1182.

(2) Zhang, Z.; Edme, K.; Lian, S.; Weiss, E. A. Enhancing the Rate of Quantum-Dot-Photocatalyzed Carbon−Carbon Coupling by Tuning the Composition of the Dot's Ligand Shell. *J. Am. Chem. Soc.* **2017**, *139* (12), 4246−4249.

(3) Bennett, T. D.; Cheetham, A. K.; Fuchs, A. H.; Coudert, F.-X. Interplay between Defects, Disorder and Flexibility in Metal-Organic Frameworks. *Nat. Chem.* **2017**, *9*, 11.
(4) Sholl, D. S.; Lively, R. P. Defects in Metal−Organic Frameworks: Challenge or Opportunity? *J. Phys. Chem. Lett.* **2015**, *6* (17), 3437−3444.
(5) Raos, G.; Idé, J. Impact of Interaction Strength and Surface Heterogeneity on the Dynamics of Adsorbed Polymers. *ACS Macro Lett.* **2014**, *3* (8), 721−726.
(6) Nguyen, H. K.; Sugimoto, S.; Konomi, A.; Inutsuka, M.; Kawaguchi, D.; Tanaka, K. Dynamics Gradient of Polymer Chains near a Solid Interface. *ACS Macro Lett.* **2019**, *8* (8), 1006−1011.
(7) Schrader, A. M.; Monroe, J. I.; Sheil, R.; Dobbs, H. A.; Keller, T. J.; Li, Y.; Jain, S.; Shell, M. S.; Israelachvili, J. N.; Han, S. Surface Chemical Heterogeneity Modulates Silica Surface Hydration. *Proc. Natl. Acad. Sci. U. S. A.* **2018**, *115* (12), 2890−2895.
(8) Garlyyev, B.; Fichtner, J.; Piqué, O.; Schneider, O.; Bandarenka, A. S.; Calle-Vallejo, F. Revealing the Nature of Active Sites in Electrocatalysis. *Chem. Sci.* **2019**, *10* (35), 8060−8075.
(9) Dubau, L.; Nelayah, J.; Asset, T.; Chattot, R.; Maillard, F. Implementing Structural Disorder as a Promising Direction for Improving the Stability of PtNi/C Nanoparticles. *ACS Catal.* **2017**, *7* (4), 3072−3081.
(10) Ye, G.; Gong, Y.; Lin, J.; Li, B.; He, Y.; Pantelides, S. T.; Zhou, W.; Vajtai, R.; Ajayan, P. M. Defects Engineered Monolayer MoS2 for Improved Hydrogen Evolution Reaction. *Nano Lett.* **2016**, *16* (2), 1097−1103.
(11) Hemminger, J. C.; Sarrao, J.; Crabtree, G.; Flemming, G.; Ratner, M. *Challenges at the Frontiers of Matter and Energy: Transformative Opportunities for Discovery Science* **2015**, DOI: 10.2172/1283188.
(12) Jain, A.; Ulijn, R. V. Restoring Order. *Nat. Chem.* **2020**, *12*, 428.
(13) Jensen, D. S.; Kanyal, S. S.; Madaan, N.; Hancock, J. M.; Dadson, A. E.; Vail, M. A.; Vanfleet, R.; Shutthanandan, V.; Zhu, Z.; Engelhard, M. H.; Linford, M. R. Multi-Instrument Characterization of the Surfaces and Materials in Microfabricated, Carbon Nanotube-Templated Thin Layer Chromatography Plates. An Analogy to 'The Blind Men and the Elephant.'. *Surf. Interface Anal.* **2013**, *45* (8), 1273−1282.
(14) Toh, C.-T.; Zhang, H.; Lin, J.; Mayorov, A. S.; Wang, Y.-P.; Orofeo, C. M.; Ferry, D. B.; Andersen, H.; Kakenov, N.; Guo, Z.; Abidi, I. H.; Sims, H.; Suenaga, K.; Pantelides, S. T.; Özyilmaz, B. Synthesis and Properties of Free-Standing Monolayer Amorphous Carbon. *Nature* **2020**, *577* (7789), 199−203.
(15) Caro, M. A.; Aarva, A.; Deringer, V. L.; Csányi, G.; Laurila, T. Reactivity of Amorphous Carbon Surfaces: Rationalizing the Role of Structural Motifs in Functionalization Using Machine Learning. *Chem. Mater.* **2018**, *30* (21), 7446−7455.
(16) Carey, J. D.; Silva, S. R. P. Disorder, Clustering, and Localization Effects in Amorphous Carbon. *Phys. Rev. B: Condens. Matter Mater. Phys.* **2004**, *70* (23), 235417.
(17) Lee, K. A. B. Electron Transfer into Self-Assembling Monolayers on Gold Electrodest. *Langmuir* **1990**, *6* (3), 709−712.
(18) Chidsey, C. E. D.; Bertozzi, C. R.; Putvinski, T. M.; Mujsce, A. M. Coadsorption of Ferrocene-Terminated and Unsubstituted Alkanethiols on Gold: Electroactive Self-Assembled Monolayers. *J. Am. Chem. Soc.* **1990**, *112* (11), 4301−4306.
(19) Finklea, H. O.; Hanshew, D. D. Electron-Transfer Kinetics in Organized Thiol Monolayer with Attached Pentaamine(Pyridine) Ruthenium Redox Centers. *J. Am. Chem. Soc.* **1992**, *114* (4), 3173−3181.
(20) Ruther, R. E.; Cui, Q.; Hamers, R. J. Conformational Disorder Enhances Electron Transfer through Alkyl Monolayers: Ferrocene on Conductive Diamond. *J. Am. Chem. Soc.* **2013**, *135* (15), 5751−5761.
(21) Meziane, D.; Barras, A.; Kromka, A.; Houdkova, J.; Boukherroub, R.; Szunerits, S. Thiol-Yne Reaction on Boron-Doped Diamond Electrodes: Application for the Electrochemical Detection of DNA-DNA Hybridization Events. *Anal. Chem.* **2012**, *84* (1), 194−200.
(22) Das, M. R.; Wang, M.; Szunerits, S.; Gengembre, L.; Boukherroub, R. Clicking Ferrocene Groups to Boron-Doped Diamond Electrodes. *Chem. Commun.* **2009**, *19*, 2753−2755.
(23) Yu, S. S. C.; Downard, A. J. Photochemical Grafting and Activation of Organic Layers on Glassy Carbon and Pyrolyzed Photoresist Films. *Langmuir* **2007**, *23*, 4662−4668.
(24) Evrard, D.; Lambert, F.; Policar, C.; Balland, V.; Limoges, B. Electrochemical Functionalization of Carbon Surfaces by Aromatic Azide or Alkyne Molecules: A Versatile Platform for Click Chemistry. *Chem. - Eur. J.* **2008**, *14* (30), 9286−9291.
(25) McKenas, C. G.; Fehr, J. M.; Donley, C. L.; Lockett, M. R. Thiol−Ene Modified Amorphous Carbon Substrates: Surface Patterning and Chemically Modified Electrode Preparation. *Langmuir* **2016**, *32* (41), 10529−10536.
(26) Fehr, J. M.; McKenas, C. G.; Liu, B.; Lockett, M. R. Azide-Alkyne Click Reactions to Prepare Chemically Modified Amorphous Carbon Electrodes. *Appl. Surf. Sci.* **2019**, *480*, 1109−1115.
(27) Landis, E. C.; Hamers, R. J. Covalent Grafting of Redox-Active Molecules to Vertically Aligned Carbon Nanofiber Arrays via "Click" Chemistry. *Chem. Mater.* **2009**, *21* (4), 724−730.
(28) Fabre, B.; Pujari, S. P.; Scheres, L.; Zuilhof, H. Micropatterned Ferrocenyl Monolayers Covalently Bound to Hydrogen-Terminated Silicon Surfaces: Effects of Pattern Size on the Cyclic Voltammetry and Capacitance Characteristics. *Langmuir* **2014**, *30* (24), 7235−7243.
(29) Kang, O. S.; Bruce, J. P.; Herbert, D. E.; Freund, M. S. Covalent Attachment of Ferrocene to Silicon Microwire Arrays. *ACS Appl. Mater. Interfaces* **2015**, *7* (48), 26959−26967.
(30) Pujari, S. P.; Scheres, L.; Marcelis, A. T. M.; Zuilhof, H. Covalent Surface Modification of Oxide Surfaces Angewandte. *Angew. Chem., Int. Ed.* **2014**, *53*, 6322−6356.
(31) Hanna, C. M.; Sanborn, C. D.; Ardo, S.; Yang, J. Y. Interfacial Electron Transfer of Ferrocene Immobilized onto Indium Tin Oxide through Covalent and Noncovalent Interactions. *ACS Appl. Mater. Interfaces* **2018**, *10* (15), 13211−13217.
(32) Li, C.; Ren, B.; Zhang, Y.; Cheng, Z.; Liu, X.; Tong, Z. A Novel Ferroceneylazobenzene Self-Assembled Monolayer on an ITO Electrode : Photochemical and Electrochemical Behaviors. *Langmuir* **2008**, *24*, 12911−12918.
(33) Robertson, J. Diamond-like Amorphous Carbon. *Mater. Sci. Eng., R* **2002**, *37* (4), 129−281.
(34) Sainio, S.; Nordlund, D.; Caro, M. A.; Gandhiraman, R.; Koehne, J.; Wester, N.; Koskinen, J.; Meyyappan, M.; Laurila, T. Correlation between Sp3-to-Sp2 Ratio and Surface Oxygen Functionalities in Tetrahedral Amorphous Carbon (Ta-C) Thin Film Electrodes and Implications of Their Electrochemical Properties. *J. Phys. Chem. C* **2016**, *120* (15), 8298−8304.
(35) Roth, K. M.; Yasseri, A. A.; Liu, Z.; Dabke, R. B.; Malinovskii, V.; Schweikart, K.-H.; Yu, L.; Tiznado, H.; Zaera, F.; Lindsey, J. S.; Kuhr, W. G.; Bocian, D. F. Measurements of Electron-Transfer Rates of Charge-Storage Molecular Monolayers on Si(100). Toward Hybrid Molecular/Semiconductor Information Storage Devices. *J. Am. Chem. Soc.* **2003**, *125* (2), 505−517.
(36) Lattimer, J. R. C.; Brunschwig, B. S.; Lewis, N. S.; Gray, H. B. Redox Properties of Mixed Methyl/Vinylferrocenyl Monolayers on Si(111) Surfaces. *J. Phys. Chem. C* **2013**, *117* (51), 27012−27022.
(37) Decker, F.; Cattaruzza, F.; Coluzza, C.; Flamini, A.; Marrani, A. G.; Zanoni, R.; Dalchiele, E. A. Electrochemical Reversibility of Vinylferrocene Monolayers Covalently Attached on H-Terminated p-Si(100). *J. Phys. Chem. B* **2006**, *110* (14), 7374−7379.
(38) Das, A. K.; Engelhard, M. H.; Liu, F.; Bullock, R. M.; Roberts, J. A. S. The Electrode as Organolithium Reagent: Catalyst-Free Covalent Attachment of Electrochemically Active Species to an Azide-Terminated Glassy Carbon Electrode Surface. *Inorg. Chem.* **2013**, *52* (23), 13674−13684.
(39) Stenehjem, E. D.; Ziatdinov, V. R.; Stack, T. D. P.; Chidsey, C. E. D. Gas-Phase Azide Functionalization of Carbon. *J. Am. Chem. Soc.* **2013**, *135* (3), 1110−1116.

https://dx.doi.org/10.1021/acsaem.0c01434
ACS Appl. Energy Mater. 2020, 3, 8038−8047

(40) Devadoss, A.; Chidsey, C. E. D. Azide-Modified Graphitic Surfaces for Covalent Attachment of Alkyne-Terminated Molecules by "Click" Chemistry. *J. Am. Chem. Soc.* **2007**, *129* (17), 5370−5371.
(41) Hapiot, P.; Noël, J.-M.; Fei, H.; Leroux, Y. R.; Roux, C. Efficient Covalent Modification of a Carbon Surface: Use of a Silyl Protecting Group To Form an Active Monolayer. *J. Am. Chem. Soc.* **2010**, *132* (40), 14039−14041.
(42) Hapiot, P.; McCreery, R. L.; Sayed, S. Y.; Bayat, A.; Leroux, Y.; Kondratenko, M. Bilayer Molecular Electronics: All-Carbon Electronic Junctions Containing Molecular Bilayers Made with "Click" Chemistry. *J. Am. Chem. Soc.* **2013**, *135* (35), 12972−12975.
(43) McCreery, R. L. Advanced Carbon Electrode Materials for Molecular Electrochemistry. *Chem. Rev.* **2008**, *108* (7), 2646−2687.
(44) Bard, A. J.; Faulkner, L. R. *Electrochemical Methods: Fundamentals and Applications*, 2nd ed.; Harris, D., Swain, E., Robey, C., Aiello, E., Eds.; John Wiley & Sons, Inc.: Hoboken, 2001.
(45) Laviron, E. The Use of Linear Potential Sweep Voltammetry and of A.C Voltammetry for the Study of the Surface Electrochemical Reaction of Strongly Adsorbed Systems and of Redox Modified Electrodes. *J. Electroanal. Chem. Interfacial Electrochem.* **1979**, *100*, 263−270.
(46) Vogel, Y. B.; Molina, A.; Gonzalez, J.; Ciampi, S. Quantitative Analysis of Cyclic Voltammetry of Redox Monolayers Adsorbed on Semiconductors: Isolating Electrode Kinetics, Lateral Interactions, and Diode Currents. *Anal. Chem.* **2019**, *91* (9), 5929−5937.
(47) Eckermann, A. L.; Shaw, J. A.; Meade, T. J. Kinetic Dispersion in Redox-Active Dithiocarbamate Monolayers. *Langmuir* **2010**, *26* (4), 2904−2913.
(48) Rowe, G. K.; Carter, M. T.; Richardson, J. N.; Murray, R. W. Consequences of Kinetic Dispersion on the Electrochemistry of an Adsorbed Redox-Active Monolayer. *Langmuir* **1995**, *11* (5), 1797−1806.
(49) Laviron, E.; Roullier, L. General Expression of the Linear Potential Sweep Voltammogram for a Surface Redox Reaction with Interactions between the Adsorbed Molecules Applications to Modified Electrodes. *J. Electroanal. Chem. Interfacial Electrochem.* **1980**, *115*, 65−74.
(50) Laviron, E. Surface Linear Potential Sweep Voltammetry: Equation of the Peaks for a Reversible Reaction When Interactions between the Adsorbed Molecules Are Taken into Account. *J. Electroanal. Chem. Interfacial Electrochem.* **1974**, *52* (3), 395−402.
(51) Eckermann, A. L.; Feld, D. J.; Shaw, J. A.; Meade, T. J. Electrochemistry of Redox-Active Self-Assembled Monolayers. *Coord. Chem. Rev.* **2010**, *254* (15−16), 1769−1802.
(52) Costentin, C.; Savéant, J.-M. Energy Storage: Pseudocapacitance in Prospect. *Chem. Sci.* **2019**, *10* (22), 5656−5666.
(53) Creager, S. E.; Wooster, T. T. A New Way of Using Ac Voltammetry To Study Redox Kinetics in Electroactive Monolayers. *Anal. Chem.* **1998**, *70* (20), 4257−4263.
(54) Nahir, T. M.; Bowden, E. F. The Distribution of Standard Rate Constants for Electron Transfer between Thiol-Modified Gold Electrodes and Adsorbed Cytochrome C. *J. Electroanal. Chem.* **1996**, *410* (1), 9−13.
(55) Matsuda, H.; Aoki, K.; Tokuda, K. Theory of Electrode Reactions of Redox Couples Confined to Electrode Surfaces at Monolayer Levels: Part II. Cyclic Voltammetry and Ac Impedance Measurements. *J. Electroanal. Chem. Interfacial Electrochem.* **1987**, *217* (1), 15−32.
(56) Matsuda, H.; Aoki, K.; Tokuda, K. Theory of Electrode Reactions of Redox Couples Confined to Electrode Surfaces at Monolayer Levels: Part I. Expression of the Current-Potential Relationship for Simple Redox Reactions. *J. Electroanal. Chem. Interfacial Electrochem.* **1987**, *217* (1), 1−13.
(57) Lee, L. Y. S.; Sutherland, T. C.; Rucareanu, S.; Lennox, R. B. Ferrocenylalkylthiolates as a Probe of Heterogeneity in Binary Self-Assembled Monolayers on Gold. *Langmuir* **2006**, *22* (9), 4438−4444.
(58) Davies, T. J.; Banks, C. E.; Compton, R. G. Voltammetry at Spatially Heterogeneous Electrodes. *J. Solid State Electrochem.* **2005**, *9* (12), 797−808.

https://dx.doi.org/10.1021/acsaem.0c01434
ACS Appl. Energy Mater. 2020, 3, 8038−8047